analytical chemistry

pubs.acs.org/ac Article

Highly Sensitive Photoelectrochemical Biosensor for MicroRNA-21 Based on a Dumbbell-Shaped Heterostructure AuNRs@end-TiO_2 Combined with Carbon Dots as Photosensitizers and Duplex-Specific Nuclease-Assisted Signal Amplification

Jiao Yang, Weixin Li, Longhua Guo,* Fang Luo, Bin Qiu, Zhenyu Lin,* and Lixin Wang*

Cite This: *Anal. Chem.* 2022, 94, 13575−13581 Read Online

ACCESS | Metrics & More | Article Recommendations | Supporting Information

ABSTRACT: TiO_2 was grown on both ends of gold nanorods (AuNRs) to form a dumbbell-shaped heterostructure (called AuNRs@end-TiO_2) first, and then assembled on the fluorine tin oxide (FTO) electrode surface through hydrophobic interactions to construct a concise photoelectrochemical microRNA-21 (miRNA-21, model target) biosensor using carbon dots (CDs) as photosensitizers. Hairpin probes (HPs) were fixed on the AuNRs@end-TiO_2-modified FTO electrode surface through the Au−S bond, and CDs-modified complementary DNA (CDs-cDNA) served as photosensitive probes. In the presence of the target, miRNA hybridized with the HP and triggered double-strand-specific nuclease to cleave the complementary part of the HP with miRNA, and miRNA was released, which can trigger another cycle to realize signal amplification. Many HPs were cleaved and the complementary sequence with cDNA was exposed, which can capture the photosensitive probes to the electrode surface and resulted in photocurrent enhancement. The photocurrent intensity system has a linear relationship with the logarithm of the miRNA concentration in the range of 0.1 fM to 100 pM with a low detection limit of 96 aM (S/N = 3). The biosensor has high sensitivity, good selectivity, and good reproducibility and shows satisfactory results in actual sample detection.

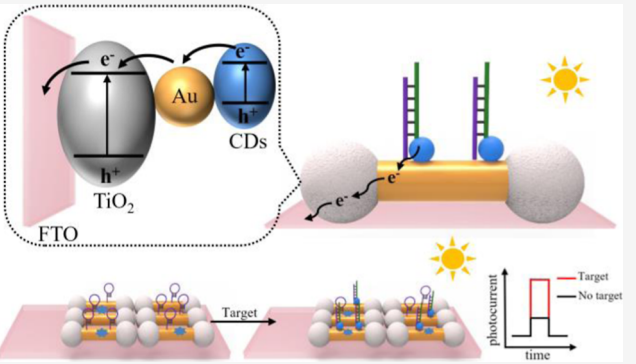

Downloaded via TSINGHUA UNIV on November 9, 2022 at 03:50:04 (UTC).
See https://pubs.acs.org/sharingguidelines for options on how to legitimately share published articles.

INTRODUCTION

Photoelectrochemical (PEC) technique is a promising means for biosensing applications with the advantages of simple equipment, low cost, and high sensitivity.[1−7] A typical PEC biosensor contains two fundamental components: (1) photoactive species to generate a PEC readout and (2) biological recognition elements to interact with the target.[8−10] Since single photoactive materials often suffer from fast electron−hole recombination or limited absorption, which lead to a low PEC response, so heterojunctions have been frequently applied to enhance the PEC signal intensity.[11−14] However, constructing heterojunctions often relies on a complex synthesis process. Biological recognition elements are important to ensure high selectivity, but classic photoactive semiconductors such as TiO_2 and ZnO lack functional groups to immobilize biomolecules.[14−16] Therefore, nanomaterials that can connect with biorecognition probes easily, such as gold nanoparticles (AuNPs) and quantum dots, are introduced frequently,[17−19] but the procedures are tedious and time-consuming. To simplify the construction procedures of PEC biosensors, it is of great significance to explore simple, heterogeneous, and multifunctional nanomaterials, which can not only generate a high PEC readout but also realize biocoupling directly.

The dumbbell-shaped heterostructures have shown good photocatalytic activity and high photoelectric conversion efficiency in the field of photocatalysis.[20,21] For example, Zhang and co-workers fabricated Fe_2O_3−TiO_2 microdumbbells with an obviously enhanced performance for PEC water oxidation. Thanks to the heterojunction between the UV-light-responsive TiO_2 and visible-light-responsive Fe_2O_3, it promoted the separation of charge carriers and enhanced the light absorption ability.[21] Wu and co-workers synthesized (gold nanorods) AuNRs/TiO_2 nanodumbbells exhibiting high photoactivity due to the intimate Schottky contact and the strong plasmonic coupling for enhanced charge separation.[22] The unique heterostructure of dumbbell-shaped AuNRs@

Received: July 25, 2022
Accepted: September 8, 2022
Published: September 20, 2022

ACS Publications © 2022 American Chemical Society

Table 1. DNA and RNA Sequences[a]

name	sequences
HP	5′-SH-TTTCGCACTAGCTTTTCAGATCAACATCAGTC
TGATAAGCTA-3′	
cDNA	5′-AGACTTAAGCTAGTGCTTTT-NH_2-3′
MiRNA-21	5′-UAGCUUAUCAGACUGAUGUUGA-3′
MiRNA-155	5′-UUAAUGCUAAUCGUGAUAGGGGU-3′
MiRNA-145	5′-UGGCAGUGUCUUAGCUGGUUGUU-3′
SM-target	5′-UAGCUUAUCAGACUGAUGUUGA-3′
TM-target	5′-UAGCUUAUCAGACUGAUGUUGA-3′

[a]The underlined letters for SM-target and TM-target are bases which differ from those in miRNA-21.

TiO_2 has good photoelectric properties and the advantage of easy functionalization, thanks to the exposed gold in the middle. In other words, the dumbbell-shaped AuNRs@TiO_2 can not only generate a high PEC signal but also immobilize DNA probes on the exposed gold part via Au−S bonds. This makes the multifunctional nanodumbbell a good candidate for constructing concise PEC biosensors, which can effectively simplify the cumbersome electrode modification procedures. However, the biosensing application of this attractive and unique dumbbell-shaped nanoparticle has rarely been reported.

Due to the wide band gap, TiO_2 can be excited only by ultraviolet (UV) light that only accounts for ∼5% of the solar spectrum. Carbon dots (CDs) have strong visible light absorption that accounts for ∼49% of the solar spectrum, which can extend the absorption range of TiO_2 to enhance the PEC signal. Thus, CDs can serve as effective photosensitizers for classic photocatalysts such as TiO_2.[23,24] For example, Gong[23] and co-workers reported that the photocurrent of the TiO_2-modified fluorine-tin oxide (FTO) electrode was greatly enhanced after loading with CDs. Cheng[24] and co-workers found a similar phenomenon because of the improved visible light absorption. Herein, microRNA-21 (miRNA-21) was chosen as a model target, and the dumbbell-shaped AuNRs@end-TiO_2 nanoparticles (NPs) were synthesized and assembled on the FTO electrode surface through hydrophobic interaction first. Hairpin probes (HP) were immobilized on the AuNRs@end-TiO_2 NP-modified electrode through the Au−S bond. CDs-modified complementary DNA (CDs-cDNA) were used as photosensitive probes to construct a sensitive PEC biosensor. The target can hybridize with HPs and lead to the digestion of the complementary part of HPs by double-strand-specific nuclease (DSN), and the target was released to start another cycle. Consequently, many HPs were nicked and the complementary sequences with cDNA were exposed, and a lot of CDs-cDNA were captured on the electrode surface, resulting in photocurrent enhancement. The proposed PEC biosensor has the advantages of simple development, high sensitivity, and good selectivity.

EXPERIMENTAL SECTION

Materials and Apparatus. The details of materials and apparatus are given in the Supporting Information. The sequences used are listed in Table 1.

Synthesis of AuNRs and Dumbbell-Shaped AuNRs@end-TiO_2. The AuNRs were synthesized according to the method reported previously.[25] AuNRs@end-TiO_2 were prepared according to a previous study with some modifications.[20] First, 20 mL of the prepared AuNR solution was centrifuged at 6010*g* and washed twice with water to remove excess cetyltrimethylammonium bromide (CTAB). Then, the AuNRs were redispersed in the mixture of 100 μL of 0.2 M CTAB solution and 20 mL of oxygen-free deionized water (solution A). Next, 100 μL of 15% titanium chloride ($TiCl_3$) solution was added into a 10 mL centrifuge tube and mixed with 2.0 mL of oxygen-free deionized water, and about 500 μL of 1.0 M sodium bicarbonate ($NaHCO_3$) was added dropwise to the $TiCl_3$ solution until the color of the mixture turned dark blue (solution B). Subsequently, 5.0 mL of solution A was added to solution B, and the mixture was gently stirred for 30 min. The obtained solution was centrifuged at 3380*g* for 10 min to collect the product and washed twice with ethanol to remove the unreacted precursor; the obtained product was dispersed in 5 mL of deionized water and kept in the dark at 4 °C for further use.

Synthesis of CDs. The water-soluble CDs were synthesized by the hydrothermal method according to a previous study;[26] see more details in the Supporting Information.

Construction of the PEC Biosensor. First, the FTO electrodes were ultrasonically cleaned with ethanol, acetone, and deionized water, respectively. The clean FTO electrodes were dried in air. Then, 30 μL of AuNRs@end-TiO_2 NP solution which had been washed to remove excess CTAB was dropped on the electrode surface and dried in air, and due to the hydrophobic interaction, the AuNRs@end-TiO_2 NPs were evenly modified on the electrode surface to form AuNRs@end-TiO_2 NPs/FTO electrodes (with an effective area of 0.3 cm^2). Next, 5.0 μL of Tween 20 solution (1.0%), 30 μL of 4.0 μM mPEG-SH solution, 6 μL of 100 μM thiolated HP (treated with TCEP to reduce disulfide bonds), and 200 μL of 3.0 M NaCl solution were mixed. The prepared AuNRs@end-TiO_2 NPs/FTO electrode was soaked in the mixed solution overnight to assemble HP on the electrode surface, and the HP/AuNRs@end-TiO_2 NPs/FTO electrode was obtained. Subsequently, the electrode was immersed in 1.0 mM MCH solution and incubated for 30 min to block non-specific binding sites. Finally, the MCH/HP/AuNRs@end-TiO_2 NPs/FTO electrode was obtained and stored at 4 °C before use.

Procedures for miRNA Detection. For standard sample detection, the prepared MCH/HP/AuNRs@end-TiO_2 NPs/FTO electrode was immersed in a standard sample (standard samples were NEBuffer 2 containing different concentrations of the target) and the electrode was incubated at 37 °C for 1 h; then, 0.5 U DSN was added for signal amplification and the electrode was incubated at 37 °C for 50 min. Afterward, the electrode was gently rinsed with buffer solution and soaked in the prepared CDs-cDNA solution for 1 h to prepare the CDs-cDNA/MCH/HP/AuNRs@end-TiO_2 NPs/FTO electrode. Finally, the obtained electrodes were gently washed with buffer solution and immersed in PBS solution for PEC tests. The PEC test used a Xe lamp as the light source, and the

https://doi.org/10.1021/acs.analchem.2c03230
Anal. Chem. 2022, 94, 13575−13581

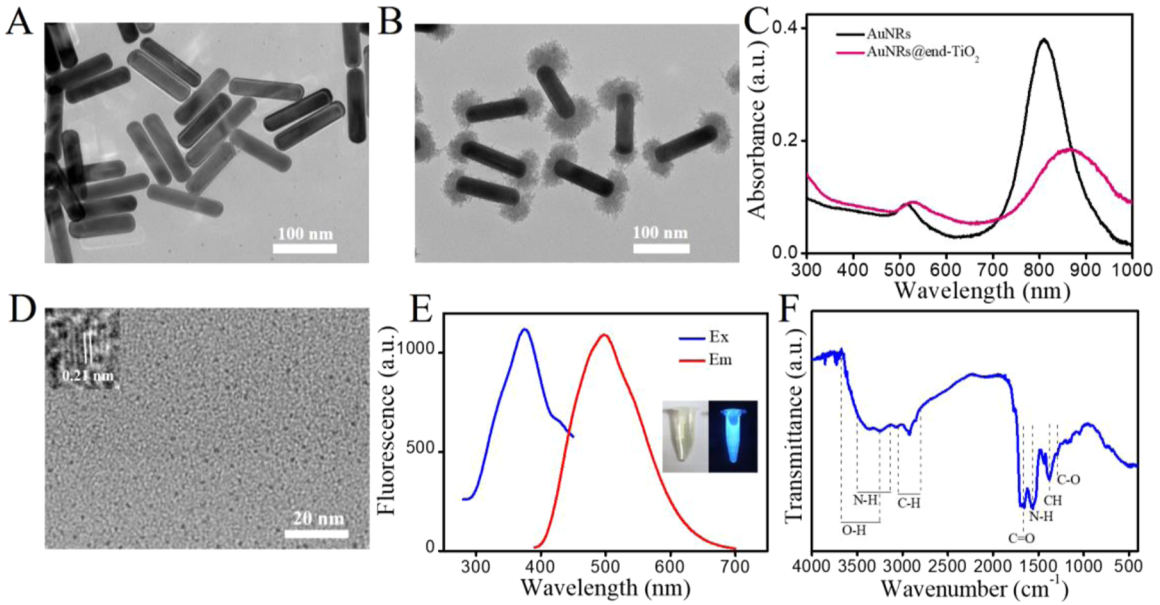

Figure 1. TEM images of (A) AuNRs and (B) AuNRs@end-TiO_2 NPs. (C) UV−vis absorption spectra of AuNRs and AuNRs@end-TiO_2 NPs. (D) TEM image of CDs, inset: HRTEM image of CDs. (E) Fluorescence spectra of CDs, inset: digital pictures under natural light and 365 nm excitation light. (F) FTIR spectrum of CDs.

Scheme 1. Schematic Illustration of the PEC Biosensor for miRNA-21 Based on AuNRs@end-TiO_2 NPs and CDs

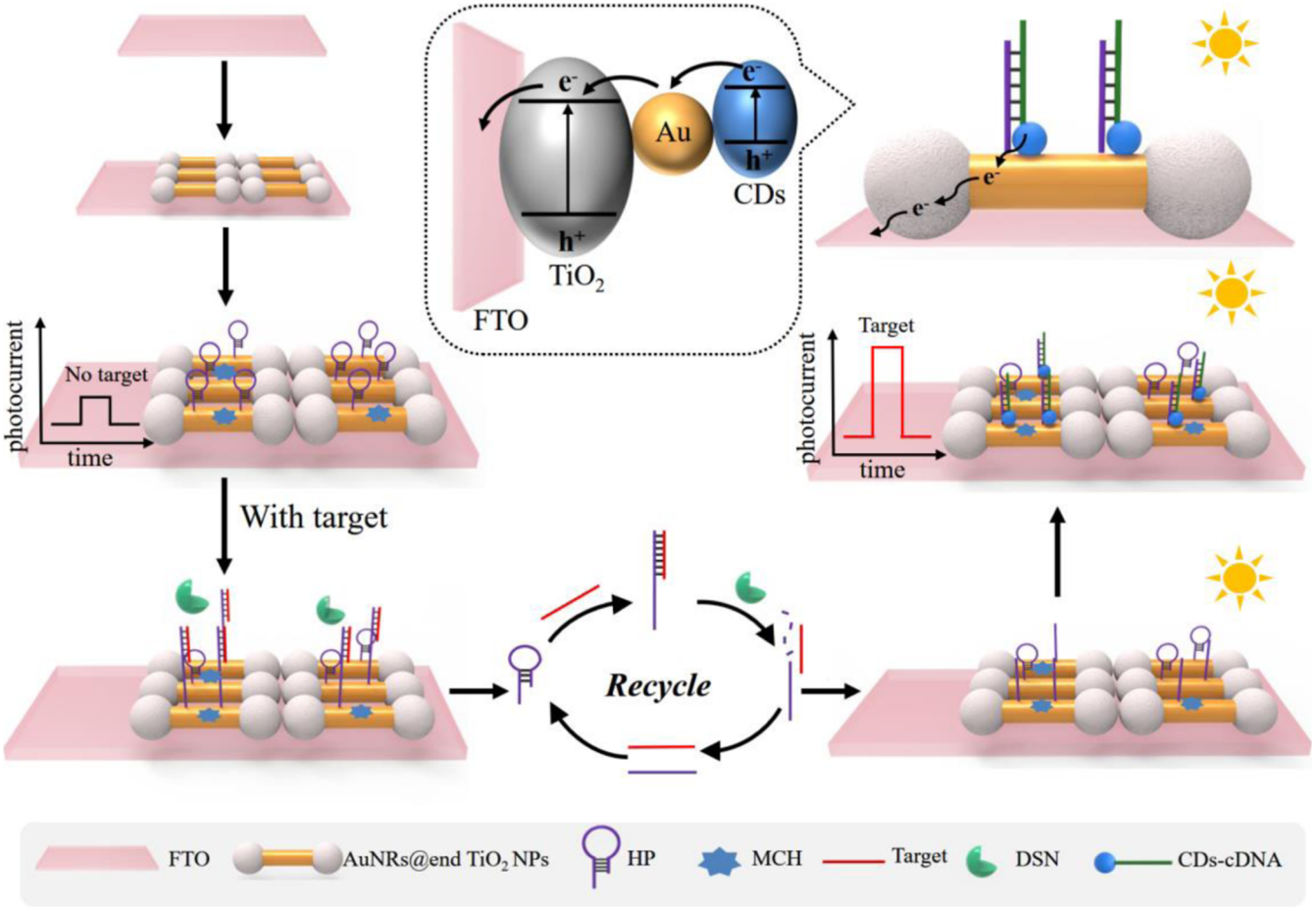

photocurrent was recorded by a electrochemical workstation with a bias voltage of 0.5 V. For real-sample detection, the total miRNA samples extracted from HeLa and MCF-7 cell lines (see more details in the Supporting Information) were utilized instead of the standard sample, and the detection procedures were the same as those used for standard sample detection.

https://doi.org/10.1021/acs.analchem.2c03230
Anal. Chem. 2022, 94, 13575−13581

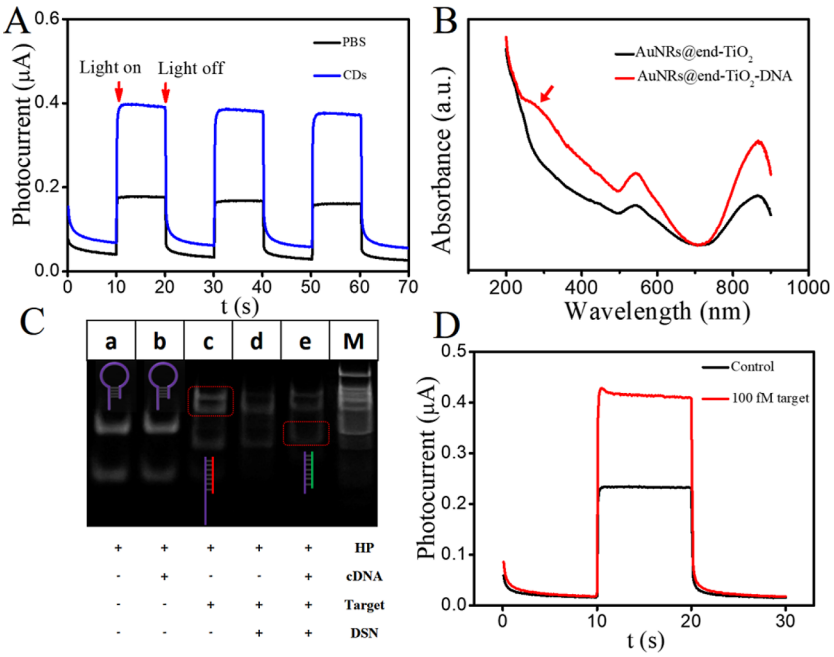

Figure 2. (A) Photocurrent response of the AuNRs@end-TiO_2-modified FTO electrode immersed in PBS buffer (black curve) and CDs solution (blue curve). (B) UV−vis absorption spectra of AuNRs@end-TiO_2 before (black curve) and after (red curve) modification with DNA probes. (C) PAGE analysis. Lane a: 2.0 μM HP, lane b: 2.0 μM HP + 2.0 μM cDNA, lane c: 2.0 μM HP + 2.0 μM target, lane d: 2.0 μM HP + 2.0 μM target + 0.5 U DSN, lane e: 2.0 μM HP + 2.0 μM target + 0.5 U DSN + 2.0 μM cDNA (cDNA was added after the deactivation of DSN), and lane M: DNA marker. (D) Photocurrent response in the absence of the target (control, black curve) and in the presence of 100 fM target (red curve).

RESULTS AND DISCUSSION

Characterization of the Prepared Nanomaterials. Transmission electron microscopy (TEM) was used to characterize the synthesized AuNRs and AuNRs@end-TiO_2 NPs. As shown in Figure 1A, the rod-shaped structure of AuNRs is about 110 nm in length and 28 nm in width. Figure 1B shows the dumbbell-shaped structure of AuNRs@end-TiO_2 NPs. TiO_2 is selectively grown on both ends of AuNRs to form good Schottky contacts.[22] The middle part of AuNRs remains naked. Figure 1C shows the ultraviolet−visible (UV−vis) absorption spectra of AuNRs and AuNRs@end-TiO_2 NPs. The black curve showed the transverse and longitudinal plasmon bands of AuNRs centered at 520 and 810 nm, respectively. After coating with TiO_2, the transverse and longitudinal plasmon bands had obvious red shifts, which was due to the refractive index change. The abovementioned results confirmed the successful synthesis of AuNRs and AuNRs@end-TiO_2.

Figure 1D shows the TEM and high-resolution TEM (HRTEM) images of CDs. The prepared CDs exhibited a uniform size of 3−5 nm, and the lattice fringes with a distance of 0.21 nm were clearly observed in the HRTEM image, which proved the successful synthesis of CDs. Figure 1E shows the fluorescence spectrum of CDs. It can be observed that the optimal excitation wavelength was ∼375 nm, and that of the emission peak (under the optimal excitation wavelength) was ∼500 nm. The digital pictures showed the color of the aqueous solution was yellow-brown, and blue fluorescence emission was observed under irradiation of UV lamp. Figure 1F displays the Fourier transform infrared (FTIR) spectrum of CDs; the stretching vibration of O−H at 3430 cm^{-1}, the stretching vibration of C−H at 2923 and 2850 cm^{-1}, and the bending vibration of N−H at 1565 cm^{-1} were observed, and the vibration absorption band of −C═O at 1670 cm^{-1} indicated that the prepared CDs are rich in carboxyl groups, nitrogen-containing functional groups, and oxygen-containing functional groups.

Principle of the Proposed PEC Biosensor for miRNA-21 Detection. As displayed in Scheme 1, AuNRs@end-TiO_2 NPs were modified on the FTO electrode surface to generate an initial photocurrent signal. HP consists of two regions: one part was complementary with cDNA, the other was complementary with the target (to avoid the hydrolyzation of HP and ensure the effect of signal amplification, the stem of the HP was well-designed and contained a one-base mismatched site, which cannot be nicked by DSN). In the absence of the target, cDNA cannot open the hairpin structure of HP, so CDs-cDNA cannot connect to the electrode surface. Therefore, a relatively low photocurrent response can be detected. In the presence of the target, the target miRNA can hybridize with HP following the principle of base complementary pairing. Since the DSN enzyme has high specificity for the DNA in the DNA-RNA duplex (DSN cannot hydrolyze HP since HP was well-designed, which had a protruding 3′-terminus and a mismatched site in the stem of the HP), the complementary part of HP in the HP-miRNA duplex was hydrolyzed by the DSN enzyme, and the target was released which participated in the next cycle. Thus, a part of HP that is complementary with miRNA was hydrolyzed, and the complementary sequence with cDNA was exposed. Thus, CDs-cDNA can connect to the electrode surface through DNA hybridization, resulting in a significant increase in photocurrent. Therefore, sensitive detection of target miRNA can be achieved by recording the change of photocurrent intensity. There may be two synergetic factors for the signal enhancement: (1) CDs have a good photosensitization effect for AuNRs@end-TiO_2 NPs due to its narrow band gap and (2) AuNRs serve as an excellent electron transporter; both CDs

https://doi.org/10.1021/acs.analchem.2c03230
Anal. Chem. 2022, 94, 13575−13581

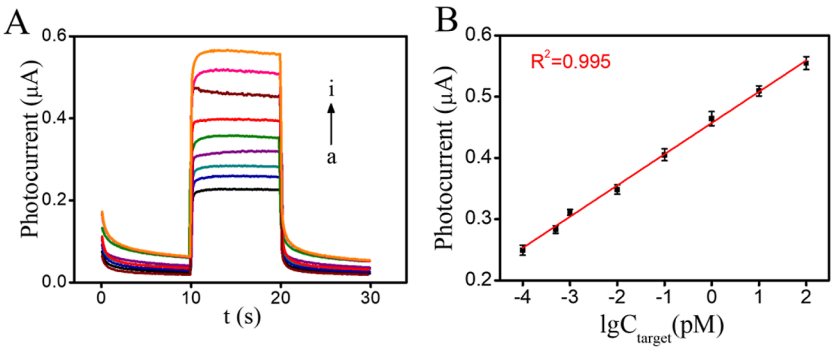

Figure 3. (A) PEC response at different concentrations of the target. (a–i): 0, 0.10 fM, 0.50 fM, 1.0 fM, 10 fM, 100 fM, 1.0 pM, 10 pM, 100 pM. (B) Relationship between the photocurrent intensities and logarithm of the target concentration in the range from 0.1 fM to 100 pM.

and TiO_2 are excited by the light source and generated photoelectrons, and the photo-electrons of CDs can be transferred to TiO_2 through AuNPs with good conductivity. The separation efficiency of electron–hole pairs was improved, and more photo-generated electrons flow to the FTO electrode to generate photocurrent.

Feasibility Study. In order to confirm the photosensitization effect of the synthesized CDs to AuNRs@end-TiO_2 NPs, the AuNRs@end-TiO_2-modified FTO electrode was immersed in PBS buffer and CDs solution for PEC tests, respectively. As shown in Figure 2A, compared with the photocurrent response measured in PBS buffer, the photocurrent intensity increased significantly when the AuNRs@end-TiO_2-modified FTO electrode was immersed in the CDs solution. The results confirmed that the CDs near the electrode surface have a good photosensitization effect on AuNRs@end-TiO_2 NPs.

To verify whether DNA probes can be modified on the dumbbell-shaped AuNRs@end-TiO_2 NPs via the Au–S bond, the UV–vis absorption spectra of the AuNRs@end-TiO_2 NPs before and after modifying with DNA probes were recorded. As shown in Figure 2B, the AuNRs@end-TiO_2 modified with DNA probes showed obvious absorption at 260 nm, which corresponded to the absorption peak of DNA, confirming that the DNA probes were successfully assembled on the surface of AuNRs@end-TiO_2 NPs via the Au–S bond.

Polyacrylamide gel electrophoresis (PAGE) characterization was carried out to verify the feasibility of the DSN enzyme-assisted cycle amplification strategy. As shown in Figure 2C, lane a and b proved that the HP cannot directly hybridize with cDNA, and lane c confirmed the successful hybridization of HP and target miRNA. The brightness of lane d became obviously darker than that of lane c, which confirmed the hydrolyzation of the complementary part of HP with the target miRNA by the DSN enzyme. Moreover, a new band appeared in lane e, confirming the hybridization of the left part of HP with cDNA. The abovementioned results indicated the feasibility of the signal amplification strategy. In addition, the feasibility of PEC biosensing was verified through a PEC control assay. As displayed in Figure 2D, in the absence of the target, a lower photocurrent was detected. When there was 100 fM target, the photocurrent enhanced significantly, which confirmed the feasibility of the constructed biosensor for target detection.

Optimization of Experimental Conditions. In order to achieve the best sensing performance, some key conditions and parameters were optimized. Since AuNRs@end-TiO_2 NPs not only served as the PEC active material but also offered the binding site for DNA probes via Au–S bonds; therefore, the dosage of AuNRs@end-TiO_2 NPs determined the initial photocurrent intensity and the number of DNA probes modified on the electrode surface. First, the volume of AuNRs@end-TiO_2 solution used to modify the FTO electrode was optimized. As shown in Figure S1A in the Supporting Information, when the volume was small, the photocurrent intensities of the control and the experimental group were relatively low. As the dosage of AuNRs@end-TiO_2 gradually increased, the photocurrent intensity of the control and the experimental group gradually increased. When the volume was more than 30 μL, the initial photocurrent was high enough, so the enhancement caused by photosensitizers was relatively weakened. Therefore, the photocurrent change value Δphotocurrent (Δphotocurrent = $I - I_0$, where I_0 is the photocurrent when there was no target, and I is the photocurrent value when there was 100 fM target) decreased, and Δphotocurrent was the highest when the volume was 30 μL. Therefore, 30 μL of AuNRs@end-TiO_2 was used for FTO electrode modification.

Sufficient capture probe HP can ensure the number of CDs-cDNA connected to the electrode surface, which ensures the sensitivity of the sensor, while excess HP may lead to steric hindrance. As displayed in Figure S1B in the Supporting Information, when the concentration of HP increased, Δphotocurrent gradually increased first and reached a plateau when the concentration of HP was 1.5 μM, which indicated 1.5 μM HP was sufficient. Therefore, the optimal concentration for HP was 1.5 μM.

Sufficient dosage and reaction time of the DSN enzyme can maximize the enzyme-assisted signal amplification efficiency, while excess dosage and reaction time of DSN may cause little nonspecific hydrolyzation, resulting in a high background. As shown in Figure S1C in the Supporting Information, as the enzyme dosage increased, the Δphotocurrent also gradually increased and reached the maximum and remained stable when the dosage increased to 0.5 U, indicating that the enzyme dosage of 0.5 U was enough. Therefore, the dosage of the DSN enzyme was determined to be 0.5 U. Similarly, as shown in Figure S1D in the Supporting Information, Δphotocurrent gradually increased with the increase of the DSN enzyme reaction time and reached a plateau when the reaction time was 50 min, so 50 min was the optimal reaction time.

Analytical Performance of the Proposed Sensor. Under the best experimental conditions, standard samples containing different concentrations of the target miRNA were used for PEC tests. As shown in Figure 3A, the photocurrent intensities gradually increased with the increase of the miRNA

https://doi.org/10.1021/acs.analchem.2c03230
Anal. Chem. 2022, 94, 13575–13581

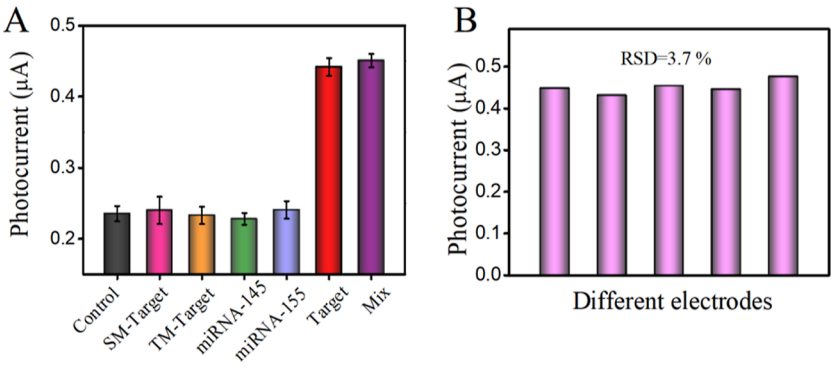

Figure 4. (A) Selectivity analysis of the proposed biosensor. The concentration of different interfering substances (SM-target, TM-target, miRNA-145, and miRNA-155) was 10 pM, the concentration of the target was 1.0 pM, and the mixture contained 1.0 pM target, 10 pM miRNA-145, and 10 pM miRNA-155. (B) Reproducibility analysis of the developed PEC biosensor in five independent tests. The target concentration was 1.0 pM.

concentration. Figure 3B shows that the photocurrent intensity and the logarithm of the miRNA concentration had a good linear relationship from 0.10 fM to 100 pM, and the linear equation could be expressed as follows

$$I\ (\mu A) = 0.051 \log C_{target}(pM) + 0.457\ (R^2 = 0.995)$$

where R is the correlation coefficient, and the limit of detection (LOD) was 96 aM (S/N = 3). As displayed in Table S1 in the Supporting Information, the analytical performance of the proposed PEC sensor was compared with other sensors for miRNA detection, and the results showed that the proposed PEC biosensor had a wider linear range and a lower LOD compared to previously studies.

In order to evaluate the selectivity and anti-interference performance of the constructed PEC sensor, several interfering substances including single-base mismatch target (SM-target), three-base mismatch target (TM-target), miRNA-145, and miRNA-155 were used for selectivity analysis. Briefly, the samples of 10 pM different interfering substances, the standard sample of 1.0 pM target miRNA, and the mixed solution containing 1.0 pM target and 10 pM miRNA-145 and miRNA-155 were used for PEC tests, respectively. As shown in Figure 4A, for 10 pM SM-target or TM-target, the increase of photocurrent was negligible. When 10 pM miRNA-145 or miRNA-155 was used for the PEC test, the photocurrent intensity had no difference with the control (NEBuffer2 with 0.5 U DSN). For the mixed solution of the target, miRNA-145, and miRNA-155, the photocurrent intensity was almost the same as that of the target only. The results indicated that the proposed biosensor had good selectivity and anti-interference. In order to explore the reproducibility of the sensor, five independent tests were performed by using five different PEC biosensors to analyze a standard sample of 1.0 pM target, and the relative standard deviation (RSD) of the photocurrent values was 3.7%, indicating that the proposed sensing platform had good reproducibility (Figure 4B). The storage stability of the proposed biosensor was evaluated. The prepared biosensor was stored at 4 °C for 10 days and used for standard sample detection. After 10 days of storage, the obtained photocurrent intensity showed no obvious difference from that of the freshly prepared biosensor, indicating that the prepared biosensor has good storage stability. Moreover, the signal stability was also investigated. After 20 cycles of on/off irradiation, 96.2% photocurrent intensity of the first cycle was retained, which indicated the good stability of the proposed biosensor.

Real-Sample Analysis. To evaluate the detection potential of the biosensor for real sample detection, a recovery experiment was carried out in 10-fold dilution of healthy human serum. The results are shown in Table S2 in the Supporting Information. The recovery rates were 103.0, 104.5, and 98.50%, respectively, and the RSD of the three independent parallel tests were 2.8, 4.1, and 3.3%, respectively. Those results proved that the sensor had good performance for miRNA detection in a complex matrix, and the sensor had the potential for real-sample detection. Finally, the constructed biosensor was applied to detect target miRNA in human breast cancer cell line (MCF-7, up-regulated level of miRNA-21) and human cervical cancer cell line (HeLa, down-regulated level of miRNA-21) lysates, respectively. The results displayed in Figure S2 in the Supporting Information showed that the photocurrent intensities increased with the increase of cell number. For the same cell number, the photocurrent intensity obtained by MCF-7 was always higher than that of HeLa. Those results indicated that the proposed biosensor has good potential for monitoring miRNA in cancer cells.

CONCLUSIONS

The multifunctional dumbbell-shaped AuNRs@end-TiO_2 NPs are used as PEC signal units to construct biosensors with the following three advantages: (1) the Schottky contact between AuNRs and TiO_2 promotes electron transfer and improves photocurrent response; (2) due to the strong plasmonic coupling of AuNRs@end-TiO_2 NPs, the charge separation was enhanced, which reduced the recombination of electron−hole pairs; (3) the exposed part of the AuNRs can directly realize the immobilization of the DNA capture probe through the Au−S bond. This unique structure not only exhibits a high photocurrent response but also simplifies the electrode modification steps. In addition, the utilization of CDs as effective photosensitizers and DSN-assisted target recycling strategy ensured the high sensitivity. This method offers a referable and common strategy for constructing simple and highly sensitive PEC biosensors.

ASSOCIATED CONTENT

Supporting Information

The Supporting Information is available free of charge at https://pubs.acs.org/doi/10.1021/acs.analchem.2c03230.

Additional experimental details including materials and apparatus, synthesis of AuNRs and CDs, cell culture, and microRNA extraction; optimization of experimental

https://doi.org/10.1021/acs.analchem.2c03230
Anal. Chem. 2022, 94, 13575−13581

conditions; and detection of miRNA-21 from HeLa and MCF-7 cell lysates (PDF)

AUTHOR INFORMATION

Corresponding Authors

Longhua Guo − *College of Biological, Chemical Sciences and Engineering, Jiaxing University, Jiaxing, Zhejiang 314001, China*; Email: guolh@zjxu.edu.cn

Zhenyu Lin − *Ministry of Education Key Laboratory for Analytical Science of Food Safety and Biology, Fujian Provincial Key Laboratory of Analysis and Detection for Food Safety, College of Chemistry, Fuzhou University, Fuzhou, Fujian 350116, China*; orcid.org/0000-0001-7890-6812; Email: zylin@fzu.edu.cn; Fax: 86-0591-22866135

Lixin Wang − *Department of Vascular Surgery, Zhongshan Xiamen Hospital, Fudan University, Xiamen 361015, China; Department of Vascular Surgery, Zhongshan Hospital, Fudan University, Shanghai 200032, China*; Phone: 86-21-64041990-2165; Email: wang.lixin@zs-hospital.sh.cn

Authors

Jiao Yang − *Ministry of Education Key Laboratory for Analytical Science of Food Safety and Biology, Fujian Provincial Key Laboratory of Analysis and Detection for Food Safety, College of Chemistry, Fuzhou University, Fuzhou, Fujian 350116, China*

Weixin Li − *Ministry of Education Key Laboratory for Analytical Science of Food Safety and Biology, Fujian Provincial Key Laboratory of Analysis and Detection for Food Safety, College of Chemistry, Fuzhou University, Fuzhou, Fujian 350116, China*

Fang Luo − *Ministry of Education Key Laboratory for Analytical Science of Food Safety and Biology, Fujian Provincial Key Laboratory of Analysis and Detection for Food Safety, College of Chemistry, Fuzhou University, Fuzhou, Fujian 350116, China*; orcid.org/0000-0003-1480-0677

Bin Qiu − *Ministry of Education Key Laboratory for Analytical Science of Food Safety and Biology, Fujian Provincial Key Laboratory of Analysis and Detection for Food Safety, College of Chemistry, Fuzhou University, Fuzhou, Fujian 350116, China*

Complete contact information is available at: https://pubs.acs.org/10.1021/acs.analchem.2c03230

Notes

The authors declare no competing financial interest.

ACKNOWLEDGMENTS

The authors gratefully acknowledge the financial support of the National Science Foundation of China (21974020).

REFERENCES

(1) Cai, Q.; Wu, D.; Li, H.; Jie, G.; Zhou, H. *Biosens. Bioelectron.* **2021**, *191*, 113455.

(2) Xu, R.; Du, Y.; Ma, H.; Wu, D.; Ren, X.; Sun, X.; Wei, Q.; Ju, H. *Biosens. Bioelectron.* **2021**, *192*, 113528.

(3) Zhou, Y.; Yin, H.; Ai, S. *Coord. Chem. Rev.* **2021**, *447*, 214156.

(4) Zhu, Q.; Li, C.; Chang, H.; Jiang, M.; Sun, X.; Jing, W.; Huang, H.; Huang, D.; Kong, L.; Chen, Z.; Sang, F.; Zhang, X. *Bioelectrochemistry* **2021**, *142*, 107928.

(5) Ge, L.; Hong, Q.; Li, H.; Liu, C.; Li, F. *Adv. Funct. Mater.* **2019**, *29*, 1904000.

(6) Zhao, Y.; Xiang, J.; Cheng, H.; Liu, X.; Li, F. *Biosens. Bioelectron.* **2021**, *194*, 113581.

(7) Song, S.; Li, N.; Bai, L.; Gai, P.; Li, F. *Anal. Chem.* **2022**, *94*, 1654−1660.

(8) Zhao, W. W.; Xu, J. J.; Chen, H. Y. *Chem. Rev.* **2014**, *114*, 7421−7441.

(9) Zhao, W. W.; Xu, J. J.; Chen, H. Y. *Chem. Soc. Rev.* **2015**, *44*, 729−741.

(10) Zhao, W. W.; Xu, J.-J.; Chen, H.-Y. *TrAC, Trends Anal. Chem.* **2016**, *82*, 307−315.

(11) Zhao, W. W.; Shan, S.; Ma, Z. Y.; Wan, L. N.; Xu, J. J.; Chen, H. Y. *Anal. Chem.* **2013**, *85*, 11686−11690.

(12) Zhao, K.; Yan, X.; Gu, Y.; Kang, Z.; Bai, Z.; Cao, S.; Liu, Y.; Zhang, X.; Zhang, Y. *Small* **2016**, *12*, 245−251.

(13) Wang, Y.; Fan, D.; Zhao, G.; Feng, J.; Wei, D.; Zhang, N.; Cao, W.; Du, B.; Wei, Q. *Biosens. Bioelectron.* **2018**, *120*, 1−7.

(14) Low, J.; Yu, J.; Jaroniec, M.; Wageh, S.; Al-Ghamdi, A. A. *Adv. Mater.* **2017**, *29*, 1601694.

(15) Wang, H.; Zhang, L.; Chen, Z.; Hu, J.; Li, S.; Wang, Z.; Liu, J.; Wang, X. *Chem. Soc. Rev.* **2014**, *43*, 5234−5244.

(16) Xu, Q.; Zhang, L.; Yu, J.; Wageh, S.; Al-Ghamdi, A. A.; Jaroniec, M. *Mater. Today* **2018**, *21*, 1042−1063.

(17) Shen, Q.; Jiang, J.; Liu, S.; Han, L.; Fan, X.; Fan, M.; Fan, Q.; Wang, L.; Huang, W. *Nanoscale* **2014**, *6*, 6315−6321.

(18) Siavash Moakhar, R.; Goh, G. K. L.; Dolati, A.; Ghorbani, M. *Electrochem. Commun.* **2015**, *61*, 110−113.

(19) Ma, Z. Y.; Ruan, Y. F.; Zhang, N.; Zhao, W. W.; Xu, J. J.; Chen, H. Y. *Chem. Commun.* **2015**, *51*, 8381−8384.

(20) Ho, K. H. W.; Shang, A.; Shi, F.; Lo, T. W.; Yeung, P. H.; Yu, Y. S.; Zhang, X.; Wong, K.-y.; Lei, D. Y. *Adv. Funct. Mater.* **2018**, *28*, 1800383.

(21) Zhang, P.; Yu, L.; Lou, X. W. *Angew. Chem., Int. Ed.* **2018**, *57*, 15076−15080.

(22) Wu, B.; Liu, D.; Mubeen, S.; Chuong, T. T.; Moskovits, M.; Stucky, G. D. *J. Am. Chem. Soc.* **2016**, *138*, 1114−1117.

(23) Gong, Y. T.; Yuan, F.; Dong, Y.; Li, Z.; Wang, G. L. *Anal. Chim. Acta* **2018**, *1014*, 19−26.

(24) Cheng, W.; Pan, J.; Yang, J.; Zheng, Z.; Lu, F.; Chen, Y.; Gao, W. *Microchim. Acta* **2018**, *185*, 263.

(25) Ye, X.; Zheng, C.; Chen, J.; Gao, Y.; Murray, C. B. *Nano Lett.* **2013**, *13*, 765−771.

(26) Zhu, S.; Meng, Q.; Wang, L.; Zhang, J.; Song, Y.; Jin, H.; Zhang, K.; Sun, H.; Wang, H.; Yang, B. *Angew. Chem., Int. Ed.* **2013**, *52*, 3953−3957.